Anal. Bioanal. Electrochem., Vol. 5, No. 2, 2013, 154 – 165

Analytical & Bioanalytical Electrochemistry

Full Paper

Electrodeposition of AuNi Alloy Nanoparticles on Mercapto Ionic Liquid–Graphite Composite Film and the Amperometric Determination of Hydroquinone

Fei Xiao, Lifeng Yang, Faqiong Zhao and Baizhao Zeng

College of Chemistry and Molecular Sciences, Wuhan University, Wuhan 430072, P R China

*Corresponding Author, Tel.:+86-27-68756626; Fax: +86-27-68754067

E-Mail: bzzeng@whu.edu.cn

Received: 27 January2013/ Accepted: 10 April 2013 / Published online: 30 April 2013

Abstract- Mercapto-imidazolium ionic liquid (IL, i.e. 1-methyl-3(2'-mercaptoacetoxyethyl) imidazolium hexafluophosphate)–graphite composite film is prepared. AuNi nanoparticles are electrodeposited on it from aqueous electrolyte. The resulting composite film coated glassy carbon electrode (AuNi–IL–graphite/GCE) is characterized by scanning electron microscopy, energy dispersive X–ray spectroscopy, X–ray diffraction and electrochemical impedance spectroscopy. The electrochemical redox of hydroquinone on the composite film is investigated. The results show that the AuNi–IL–graphite has high catalysis and stability. In neutral solutions, it can yield sensitive and stable amperometric response to hydroquinone. At 0.05 V (*vs*. SCE) the response current is linear to hydroquinone concentration in the range of 0.5–40 μM, with a detection limit of 0.05 μM (*S/N*=3) and sensitivity of 0.92 mA cm^{-2} μM^{-1}.

Keywords- AuNi Alloy Nanoparticles, Graphite, Electrodeposition, Ionic Liquid, Hydroquinone

1. INTRODUCTION

The fabrication of bimetallic nanoparticles (NPs) has attracted much attention because they have some unique physicochemical properties in comparison with monometal NPs, such

as catalytic selectivity, stability, magnetic property and corrosion resistance [1], and they are useful in electronics, photonics and catalysis [2]. The superior catalytic activity of bimetallic NPs can be attributed to two effects [3]. One is the "bifunctional effect", which is related to the geometry change of bimetallic system with respect to monometallic system; the other is the "ligand or electronic effect", which suggests that the electronic property of pure metal should be modified by the second metallic component. Various methods have been developed for the fabrication of bimetallic NPs comprising noble metal and transition metal [4]. The electrodeposition method is expected to promote the application of bimetallic NPs because it has high material efficiency and high deposition rate in comparison with typical vapor deposition [5]. Electrodeposition method also shows advantages of low cost, simple equipment and large-scale processing in comparison with other technology [6]. In our previous work several alloy NPs were fabricated by electrodeposition from aqueous electrolytes [7,8].

For effective electrodeposition of metal NPs, the supporting material should possess high electrical conductivity, good stability and large surface area [9]. Generally, carbon materials are used for such purpose. However, graphite was seldom used as support for the electrodeposition of metal NPs because crude graphite is usually agglomerate and short of appropriate linker and the metal particles deposited on its surface are exiguous.

ILs is organic salts with low melting points and they have gained wide recognition as novel solvents as they have many fascinating chemical and physical properties [10]. Their application in the synthesis of nanostructure, especially in the electrodeposition of metal NPs [11], is interesting. In particular, imidazolium ILs have been intensively studied because of their high thermal and electrochemical stability. Imidazolium ILs could form an external layer around the metal NPs to control the growth of particle size and affect the mass-transportation. Hence they are good medium for the formation and stabilization of metal NPs [12].

In this paper, AuNi alloy NPs is prepared on mercapto-imidazolium IL–graphite composite film by ultrasonic potentiostatic deposition. The IL–graphite composite has advantages of high conductivity, low interface tension, high nucleation rate and antifouling. Moreover, the imidazoliuom ring of the IL can interact with the surface of graphite [13], and the mercapto group can interact with the metal NPs. Therefore, the IL can act as a linker to connect metal NPs with graphite [14]. The obtained alloy NPs are characterized by scanning electron microscopy (SEM), energy dispersive X–ray spectroscopy (EDX), X–ray diffraction (XRD), electrochemical impedance spectroscopy (EIS) and cyclic voltammetry (CV). The electrocatalytic activity of the resulted electrode is investigated by using hydroquinone as a model molecule.

2. EXPERIMENTAL

2.1. Reagents

$HAuCl_4$, $CoSO_4$, $NiSO_4$, $CsClO_4$, *N*,*N*-dimethylformamide (DMF) and hydroquinone were purchased from Sinopharm Group Chemical Reagent Co. (Shanghai, China), and their solutions were prepared with redistilled water. The 1–methyl–3(2'–mercaptoacetoxyethyl) imidazolium hexafluophosphate was synthesized as previously reported [15]. The working solutions were prepared by diluting the stock solution with phosphate buffer solution (PBS) and water. All other chemicals used were of analytical reagent grade. The water used was redistilled.

2.2. Apparatus

Electrodeposition, EIS, CV and chronoamperometric experiments were performed with a CHI 660B electrochemical workstation (CH Instrument Company, Shanghai, China). A conventional three-electrode system was adopted. The working electrode was a modified glassy carbon electrode (3 mm in diameter) or a glass substrate (10 mm×30 mm×2.2 mm) coated with a fluorine–doped tin oxide film (FTO: 150 nm, 20 Ω), and the auxiliary and reference electrodes were a platinum wire and a saturated calomel electrode (SCE), respectively. The SEM image was obtained using a Hitachi X–650 SEM (Hitachi Co., Japan), with an EDX meter for elemental chemical analysis. XRD data were recorded with a Rigaku D/max–rA diffractometer (Japan) using Cu *K*α radiation (40 kV, 200 mA) with a Ni filter. All measurements were conducted at room temperature.

2.3. Fabrication of composite film coated electrode

The graphite was purified through refluxing in HNO_3–H_2SO_4 (volume ratio:1:3) mixture, washed with redistilled water and dried under vacuum. GCE and FTO glass were ultrasonicated in acetone, ethanol and water for 10 min each, and then were dried at room temperature. 1-Methyl-3(2'-mercaptoacetoxyethyl) imidazolium hexafluophosphate (200 μL) and graphite (10 mg) were mixed and ground in an agate mortar to prepare a uniform black gel. Then it was dispersed in 10 mL DMF, with aid of ultrasonic agitation. 10 μL of the resulting suspension was transferred on a cleaned GCE and the solvent was evaporated in air. Thus a uniform film coated electrode (IL–graphite/GCE) was obtained. IL–graphite/FTO was fabricated through a similar method. The electrochemical deposition was performed in 0.050 M $CsClO_4$+1.0 mM $HAuCl_4$, 0.050 M $CsClO_4$+1.0 mM $HAuCl_4$+1.0 mM $NiSO_4$ and 0.050 M $CsClO_4$+1.0 mM $HAuCl_4$+1.0 mM $CoSO_4$ for the preparation of Au, AuNi and AuCo NPs, respectively. During potentiostatic deposition, ultrasonic wave (45 W) irradiation was employed [16]. The deposition potential was varied from -0.5 V to -1.1 V. The obtained electrodes were washed carefully with redistilled water and then dried at room temperature.

All the electrodes were stored at room temperature by immersing in 0.10 M PBS (pH 7.4). Prior to experiments the solutions were deoxygenated with nitrogen gas.

3. RESULTS AND DISCUSSION

3.1. Characterization of alloy NPs

Fig. 1 displays the SEM images of graphite, IL–graphite, AuNi–graphite and AuNi–IL–graphite composite films. As can be seen, the purified graphite particles still agglomerate seriously (Fig. 1a); however, the surface of IL–graphite composite is more uniform and the graphite particles are better dispersed (Fig. 1b). This is because the imidazoliuom ring of IL can interact with the π–electronic surface of graphite [13]. Upon electrodeposition, the composite surface is covered by AuNi NPs. It is clear, much more NPs are deposited on IL–graphite composite than on graphite, and the particle diameters are also much smaller on IL–graphite composite. This indicates that both IL and well dispersive graphite particles can promote the deposition of AuNi NPs. IL can form two-dimensional polymeric structure due to the hydrogen bond between the cation and anion, and so it is reasonable to deduce that IL may act as template for the formation of NPs [17]. In addition, the –SH group of the IL also benefits the deposition of AuNi NPs as it can interact with metal particles. Therefore, the IL also acts as a linker to connect metal NPs with graphite in this case.

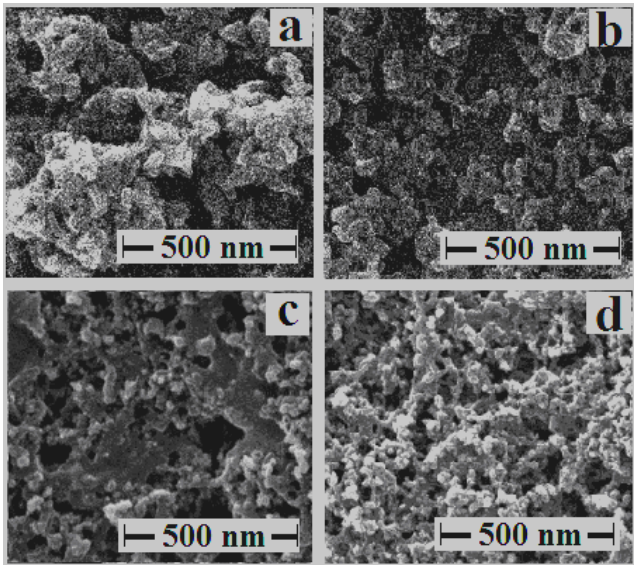

Fig. 1. SEM images of purified graphite (a), IL–graphite (b), AuNi–graphite (c) and AuNi IL–graphite (d). Electrodeposition potential: -1.1 V (*vs*. SCE); electrodeposition time: 500 s

The EIS of different electrodes in $[Fe(CN)_6]^{3-/4-}$ solution are recorded (Fig. 2). The shape of Nyquist plot for all the electrodes studied is a semicircle plus a straight line. The semicircle for the bare GCE is bigger and the electron transfer resistance is higher (R_{ct}=655 Ω), whereas, the resistance of graphite/GCE (R_{ct}=463 Ω) is smaller. The IL–graphite/GCE exhibits an even smaller electron transfer resistance (R_{ct}=357 Ω). This is closely related to the effect of conductive IL and the improved dispersion of graphite particles. When the electrode is coated with AuNi NPs the electron transfer resistance decreases markedly (R_{ct}=205 Ω). This is because metal NPs have good conductivity and can provide necessary conductive pathways for electron transfer.

Fig. 2 shows the CVs of AuNi NPs deposited on different supports in deaerated H_2SO_4 solutions. The CVs are similar to that of polycrystalline Au, showing the typical oxide formation peak and associated stripping peak. This indicates that the electrode is covered by Au. The electroactive Au surface area (S_{EAS}) can be estimated according to the charge corresponding to the stripping of Au surface oxide (420 μC cm^{-2}) [18]. As shown in Table 1, the S_{EAS} for AuNi deposited on IL–graphite film is bigger than that on graphite support. It is due to the well dispersion of graphite particles and the high substrate coverage of AuNi on IL–graphite. Moreover, the S_{EAS} of AuNi particles increases with electrodeposition potential decreasing, indicating that the deposition of alloy particles is more effective at sufficiently negative potential.

Fig. 3 presents the XRD patterns of Au and AuNi NPs deposited on IL–graphite composite film. The broad reflection peak observed at 2θ=25° is generated by graphite support. The other four peaks are characteristic peak of face centered cubic (fcc) crystalline Au (JCPDS–ICDD, Card No. 04–0784), corresponding to the planes (111), –(200), –(220) and –(311) at 2θ values of about 38.18, 44.29, 64.23 and 77.43°, respectively. This indicates that the alloy NPs have principally single–phase disordered structure. Compared with the peaks of pure Au, the diffraction peaks of AuNi shift slightly to higher 2θ values, this reveals that Ni has entered into the Au lattice and an alloy of Au and Ni forms. Additionally, small amount of pure Ni or oxides/hydroxides phase is evidenced by diffraction pattern shoulders at 43° and 59° for AuNi. For comparison, AuCo NPs are deposited under the conditions, and similar phenomenon is observed (Fig. 3). The average size of alloy particles is estimated by using the Scherrer equation [19]: L=0.9 $\lambda k_{a1}/B_{(2\theta)}\cos\theta_B$, where L is the average size of particles, λk_{a1} the X–ray wavelength, $B_{(2\theta)}$ the peak broadening, and θ_B the angle of the peak maximum. The average particle sizes calculated for Au, AuCo and AuNi are 31.5, 25.8 and 20.5 nm, respectively, meaning that the alloying of Au with non-precious metal can lower the grain size effectively. This is because small amount of Ni (or Co) or oxides/hydroxides may cover the alloy NPs to restrain their growth during the electrodeposition. However, the average size of alloy particles increases with potential decreasing as shown in Table 1.

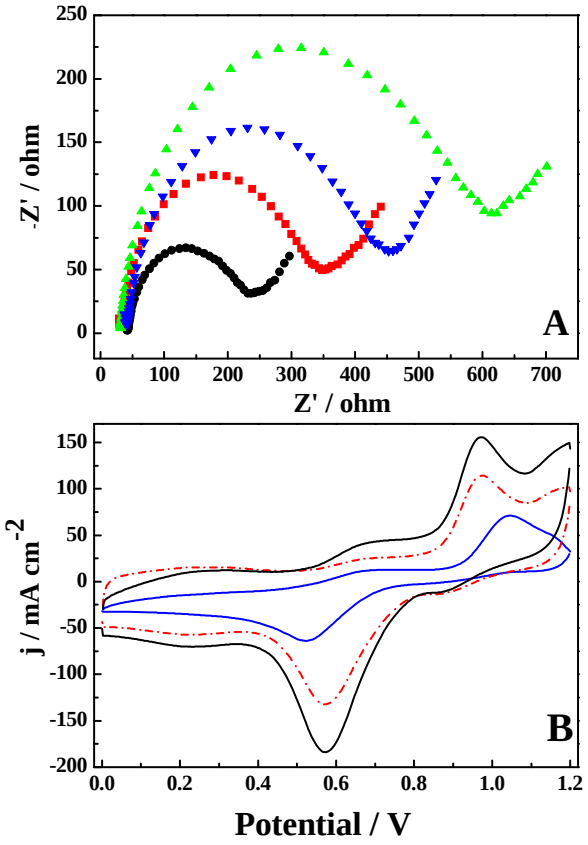

Fig. 2. (A) Nyquist plots of bare GCE, graphite/GCE, IL–graphite/GCE, AuNi/IL–graphite/GCE (from outer to inner). Solution composition: 1.0 mM $K_3Fe(CN)_6$+1.0 mM $K_4Fe(CN)_6$+0.1 M KCl; frequency range: 0.1–10^5 Hz. (B) CVs of AuNi/GCE, AuNi/graphite/GCE and AuNi/IL–graphite/GCE (from inner to outer). Supporting electrolyte: 0.5 M H_2SO_4; potential scan rate: 100 mV s^{-1}

Assuming the validity of Vegard's Law (the linear lattice constant–concentration relation) [20], one can estimate the composition of the alloys. The results are shown in Table 1. For comparison, the EDX analysis is also carried out (Table 1). As can be seen, there are systematic discrepancies between the alloy composition estimated according to Vegard's Law and EDX. This inconsistency may be caused by deviation from linearity of the lattice constant–composition relation. In addition, XRD analysis refers only to the crystalline part of the sample, while EDX characterizes the entire sample. With this in mind, the XRD and EDX data can be reconciled, provided the as prepared alloy comprises both ordered crystalline and disordered (amorphous) regions enriched with transition metals [21]. Both XRD and EDX results indicate that the Au content in the film decreases with electrodeposition potential

moving negatively. Therefore, we could conclude that the effect of potential on electrodeposition is prominent.

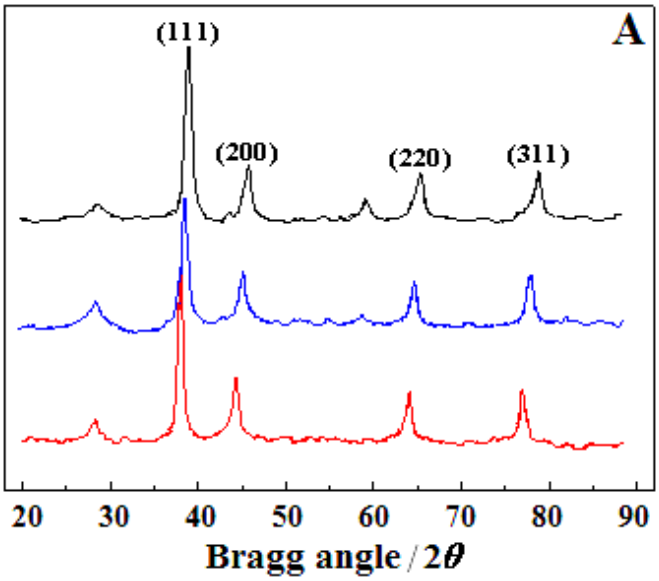

Fig. 3. XRD patterns of AuNi, AuCo and Au NPs (from upper to bottom) deposited on IL–graphite film

Table 1. Surface area of alloy NPs calculated according to CV and composition of alloy NPs estimated from XRD and EDX analysis

Electrodes	Electrodeposition potential	S_{EAS}	d_{XRD} (nm)	Composition of alloy (atomic ratio)	
				XRD	EDX
AuNi/GCE	-1.1	0.11	-	-	-
AuNi–graphite/GCE	-1.1	0.35	-	-	-
AuNi–IL–graphite/GCE	-1.1	0.47		-	-
Au–IL–graphite/GCE	-1.1	0.39	31.5	-	-
AuCo–IL–graphite/GCE	-1.1	0.45	25.8	$Au_{80}Co_{20}$	$Au_{82}Co_{18}$
AuNi–IL–graphite/GCE	-1.1	0.47	20.5	$Au_{69}Ni_{31}$	$Au_{75}Ni_{25}$
AuNi–IL–graphite/GCE	-0.5	0.29	18.2	$Au_{90}Ni_{10}$	$Au_{93}Ni_{7}$
	-0.7	0.32	18.6	$Au_{85}Ni_{15}$	$Au_{87}Ni_{13}$
	-0.9	0.43	19.3	$Au_{71}Ni_{29}$	$Au_{79}Ni_{21}$
	-1.1	0.47	20.5	$Au_{69}Ni_{31}$	$Au_{75}Ni_{25}$

3.2. Electrochemical catalysis of AuNi/IL–graphite/GCE towards hydroquinone

The voltammetric behavior of hydroquinone at different electrodes is compared (Fig. 4). Hydroquinone exhibits irreversible redox peaks at the bare GCE, and the peak current density (j_p) is small. Under identical conditions, hydroquinone yields a pair of quasi–reversible peaks at the graphite/GCE. As can be seen, the IL–graphite/GCE exhibits better catalysis to hydroquinone: j_p increases and peak separation (ΔE_p) decreases. After the electrodeposition of AuNi, the resulting AuNi/GCE, AuNi–graphite/GCE and AuNi–IL–graphite/GCE show better electrocatalysis for hydroquinone redox. This should be ascribed to the promotion of nanometal to electron-transfer and the enhanced electrode area. The electrochemical reaction of hydroquinone is almost reversible at AuNi–graphite/GCE and AuNi–IL–graphite/GCE. For different electrodes the value of j_p follows the order of j_p (AuNi/GCE)<j_p (AuNi–graphite/GCE) < j_p (AuNi–IL–graphite/GCE), which is closely related to their S_{EAS}.

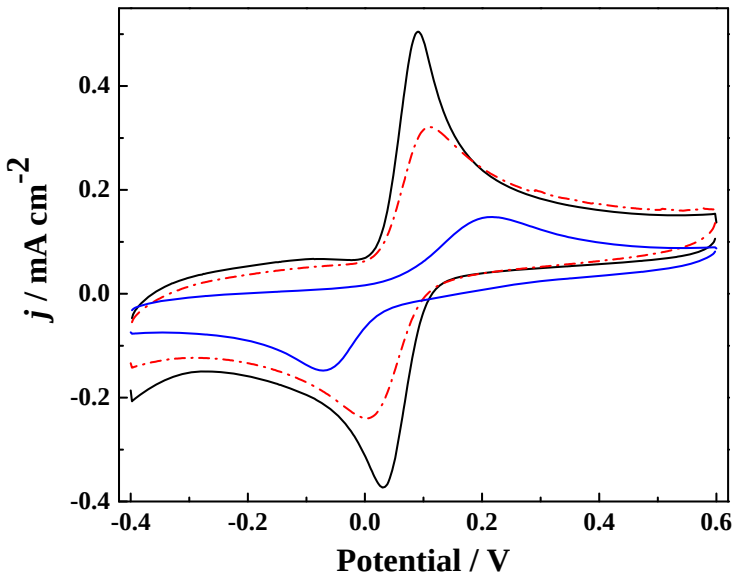

Fig. 4. CVs of AuNi/GCE, AuNi–graphite/GCE and AuNi–IL–graphite/GCE (from inner to outer). Solution composition: 0.10 M PBS (pH=7.4)+50 μM hydroquinone; potential scan rate: 100 mV s^{-1}

The amperometric response of different electrodes to hydroquinone at 0.05 V is compared to determine the optimal composition of alloy for hydroquinone sensing. As shown in Fig. 5, the Au–IL–graphite/GCE presents weak response to hydroquinone, while the AuCo–IL–graphite/GCE and AuNi–IL–graphite/GCE show sensitive current response; furthermore, their response is stable and repeatable. These reveal that the introduction of Co

and Ni improves both electrocatalytic activity and stability. Among them AuNi–IL–graphite/GCE presents more sensitive amperometric response in this case.

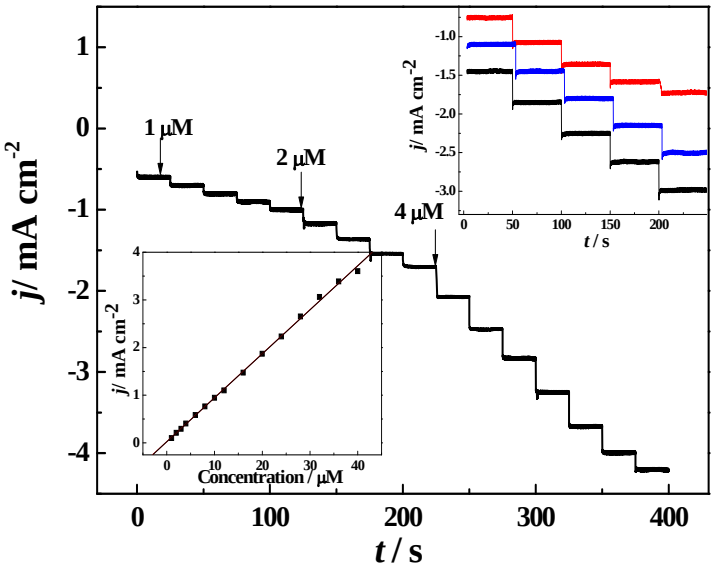

Fig. 5. Typical amperometric response of AuNi–IL–graphite/GCE to successive addition of 1 μM, 2 μM and 4 μM hydroquinone in a stirred PBS (pH=7.4). Applied potential: 0.05 V. Inset: calibration curve for the amperometric response of AuNi–IL–graphite/GCE to hydroquinone (left), and the amperometric response of Au–IL–graphite/GCE, AuCo–IL–graphite/GCE and AuNi–IL–graphite/GCE to successive addition of 4 μM hydroquinone (right, from upper to bottom)

To optimize the fabrication conditions of AuNi–IL–graphite/GCE, the influence of deposition potential is examined. With the deposition potential changing from -0.5 to -1.1 V, the response current increases. At -1.1 V, the resulting electrode presents larger response current. The deposition potential is hence fixed at –1.1 V.

The current–time plot and calibration curve for the AuNi–IL–graphite/GCE are also depicted in Fig. 5. The response current is linear to hydroquinone concentration in the range of 0.5–40 μM, with a detection sensitivity of 0.92 mA cm^{-2} μM^{-1}; the detection limit is 0.05 μM (*S/N*=3). The sensitivity is higher and the linear range is wider in comparison with those of carbon ionic liquid electrode, cobalt hydroxide film coated electrode, poly (diallyldimethylammonium chloride) functionalized graphene-modified glassy carbon electrode and electrospun carbon nanofiber modified electrode [22-25].

The repeatability and stability of the electrode is evaluated. A 10 μM hydroquinone solution is measured successively for ten times at 0.05 V using a electrode, the relative standard deviation (RSD) of response current is 4.3%. The store-stability of AuNi–IL–

graphite/GCE at room temperature is investigated by recording its current response to 10 μM hydroquinone. It retains about 94% of its initial sensitivity after 28 days.

3.3. Determination of hydroquinone in lake water

The AuNi–IL–graphite/GCE is applied to the determination of hydroquinone in lake water. A standard addition method is adapted to estimate the accuracy. Here, 9.0 mL water sample and 1.0 mL of 1.0 M PBS (pH=7.4) are mixed for determination, and the results obtained as mean of five repetitious measurements are shown in Table 2. The recoveries for the standards added are 94.7–107.8%.

Table 2. Measurement results of hydroquinone in lake water samples

Samples	Added (μM)	Found (μM)	Recovery (%)
1	0.0	0.57	-
	1.0	1.68	107
	5.0	5.85	105
2	0.0	ND[a]	-
	5.0	5.39	108
	10.0	9.83	98
3	0.0	ND	-
	10.0	9.47	95
	20.0	19.2	96

[a]: not detected

4. CONCLUSIONS

A mercapto IL-graphite composite was fabricated by grinding. Well dispersive AuNi NPs could be electrodeposited on the IL–graphite composite film. The NPs exhibited the features of alloy. The AuNi–IL–graphite coated GCE presented small electron transfer resistance and big electroactive surface area. In neutral solutions, it exhibited high electrocatalysis to hydroquinone. At 0.05 V the electrode could yield sensitive, stable and repeatable amperometric response to hydroquinone, thus it can be used to detect hydroquinone concentration.

Acknowledgement

The authors appreciate the support from the National Natural Science Foundation of China (Grant No.:21075092) and the State Key Laboratory of Advanced Technology for

Materials Synthesis and Processing (Wuhan University of Technology, Grant No. 2010-KF-12).

REFERENCES

[1] D. Lu, K. Domen, and K. Tanaka, Langmuir 18 (2002) 3226.
[2] S. Zhou, Z. Ma, H. Yin, Z. Wu, B. Eichhorn, S. H. Overbury, and S. Dai, J. Phys. Chem. C 113 (2009) 5758.
[3] E. Florez, F. Mondragon, and P. Fuentealba, J. Phys. Chem. B 110 (2006) 13793.
[4] F. H. B. Lima, W. H. Lizcano–Valbuena, E. Teixeira–Neto, F. C. Nart, E. R. Gonzalez, and E. A. Ticianelli, Electrochim. Acta 52 (2006) 385.
[5] N. Fujita, S. Maeda, S. Yoshida, M. Takase, M. Nakano, and H. Fukunaga, J. Magn. Magn. Mater. 272 (2004) E1895.
[6] S. Z. Chu, S. Inoue, K. Wada, and K. Kurashima, J. Phys. Chem. B 108 (2004) 5582.
[7] F. Xiao, Z. R. Mo, F. Q. Zhao, and B. Z. Zeng, Electrochem. Commun. 10 (2008) 1740.
[8] F. Xiao, F. Q. Zhao, Y. F. Zhang, G. P. Guo, and B. Z. Zeng, J. Phys. Chem. C 113 (2009) 849.
[9] C. Yang, D. Wang, X. Hua, C. Dai, and L. Zhang, J. Alloy Compd. 448 (2008) 109.
[10] O. Raz, G. Cohn, W. Freyland, O. Mann, and Y. Ein–Eli, Electrochim. Acta 54 (2009) 6042.
[11] A. Safavi, N. Maleki, F. Farjami, and E. Farjami, J. Electroanal. Chem. 626 (2009) 75.
[12] K. Biswas, and C. N. R. Rao, Chem. Eur. J. 13 (2007) 6123.
[13] H. Zhang, and H. Cui, Langmuir 25 (2009) 2604.
[14] T. Fukushima, A. Kosaka, Y. Ishimura, T. Yamamoto, T. Takigawa, N. Ishii, and T. Aida, Science 300 (2003) 2072.
[15] S. Gao, H. Zhang, X. Wang, W. Mai, C. Peng, and L. Ge, Nanotechnology 16 (2005) 1234.
[16] F. Xiao, F. Q. Zhao, and B. Z. Zeng, Electrochem. Commun. 12 (2010) 611.
[17] H. Chen, and S. Dong, Langmuir 23 (2007) 12503.
[18] H. Kita, and H. Nakajima, Electrochim. Acta 31(1986) 193.
[19] V. Ponec, and G. C. Bond, Catalysis by Metals and Alloys, Elsevier Science Pub. Co. (1995).
[20] H. P. Klug, and L. E. Alexander, X-Ray Diffraction Procedures for Polycrystalline and Amorphous Materials (2nd ed.), Wiley, New York (1974).
[21] N. Travitsky, T. Ripenbein, D. Golodnitsky, Y. Rosenberg, L. Burshtein, and E. Peled, J. Power. Sources 161 (2006) 782.
[22] A. Safavi, N. Maleki, and F. Tajabadi, Analyst 132 (2007) 54.
[23] Y. Zhang, and J. B. Zheng, Electrochim. Acta 52 (2007) 7210.

[24] L. T. Wang, Y. Zhang, Y. L. Du, D. B. Lu, Y. Z. Zhang, and C. M. Wang, J. Solid State Electrochem. 16 (2012) 1323.

[25] Q. H.Guo, J. S. Huang, P. Q. Chen, Y. Liu, H. Q. Hou, and T. Y. You, Sens. Actuator B Chem. 163 (2012) 179.